8-2007

Molecular Determinants of Mg2+ and Ca2+ Permeability and pH Sensitivity in TRPM6 and TRPM7*s

Mingjiang Li
University of Connecticut School of Medicine and Dentistry

Jianyang Du
University of Connecticut School of Medicine and Dentistry

Jianmin Jiang
University of Connecticut School of Medicine and Dentistry

William J. Ratzan
University of Connecticut School of Medicine and Dentistry

Li-Ting Su
University of Medicine and Dentistry of New Jersey-Robert Wood Johnson Medical School

See next page for additional authors

Published in final edited form as:
J Biol Chem. 2007 August 31; 282(35): 25817–25830. doi:10.1074/jbc.M608972200.

Molecular Determinants of Mg^{2+} and Ca^{2+} Permeability and pH Sensitivity in TRPM6 and TRPM7[s*]

Mingjiang Li[‡,1,2], **Jianyang Du**[‡,1], **Jianmin Jiang**[3,‡], **William Ratzan**[‡], **Li-Ting Su**[§], **Loren W. Runnels**[§], and **Lixia Yue**[‡,4]

[‡]Center for Cardiology and Cardiovascular Biology, Department of Cell Biology, University of Connecticut Health Center, Farmington, Connecticut 06030

[§]Department of Pharmacology, University of Medicine and Dentistry of New Jersey-Robert Wood Johnson Medical School, Piscataway, New Jersey 08854

Abstract

The channel kinases TRPM6 and TRPM7 have recently been discovered to play important roles in Mg^{2+} and Ca^{2+} homeostasis, which is critical to both human health and cell viability. However, the molecular basis underlying these channels' unique Mg^{2+} and Ca^{2+} permeability and pH sensitivity remains unknown. Here we have created a series of amino acid substitutions in the putative pore of TRPM7 to evaluate the origin of the permeability of the channel and its regulation by pH. Two mutants of TRPM7, E1047Q and E1052Q, produced dramatic changes in channel properties. The I–V relations of E1052Q and E1047Q were significantly different from WT TRPM7, with the inward currents of 8- and 12-fold larger than TRPM7, respectively. The binding affinity of Ca^{2+} and Mg^{2+} was decreased by 50- to 140-fold in E1052Q and E1047Q, respectively. Ca^{2+} and Mg^{2+} currents in E1052Q were 70% smaller than those of TRPM7. Strikingly, E1047Q largely abolished Ca^{2+} and Mg^{2+} permeation, rendering TRPM7 a monovalent selective channel. In addition, the ability of protons to potentiate inward currents was lost in E1047Q, indicating that E1047 is critical to $Ca^{2+}$and Mg^{2+} permeability of TRPM7, and its pH sensitivity. Mutation of the corresponding residues in the pore of TRPM6, E1024Q and E1029Q, produced nearly identical changes to the channel properties of TRPM6. Our results indicate that these two glutamates are key determinants of both channels' divalent selectivity and pH sensitivity. These findings reveal the molecular mechanisms underpinning physiological/pathological functions of TRPM6 and TRPM7, and will extend our understanding of the pore structures of TRPM channels.

TRPM6 and TRPM7 belong to the TRP channel superfamily (1–5) and are distinguished from other known ion channels by virtue of having both ion channel and protein kinase activities (6–11). In addition, TRPM6 and TRPM7 uniquely exhibit strong outward rectification, permeation to Ca^{2+}, Mg^{2+}, monovalent cations, and a wide array of trace metals (6–8, 11, 12). The channel activity of TRPM7 is regulated by intracellular Mg^{2+}(7) and other divalent cations (13–15), Mg^{2+}-ATP (7, 12, 16), phosphatidylinositol 4,5-bisphosphate (14, 17), cAMP (18), and internal and external pH conditions (14, 19). Similarly, TRPM6 channel activities have been shown to be inhibited by intracellular Mg^{2+} and potentiated by external protons (8, 11). Recent studies have demonstrated that TRPM6

*This work was supported by American Heart Association Grant 0335124N and National Institutes of Health Grant HL078960 (to L. Y.).

[s]The on-line version of this article (available at http://www.jbc.org) contains supplemental Tables S1 and S2 and Fig. S1.

[4]To whom correspondence should be addressed. Tel.: 860-679-3869; Fax: 860-679-1426; lyue@uchc.edu.
[1]Both authors contributed equally to this work.
[2]Present address: Dept. of Cardiology, Renmin Hospital of Wuhan University, Peoples Republic of China.
[3]Present address: Dept. of Pharmacology and Toxicology, Sun Yat-Sen University, Peoples Republic of China.

and TRPM7 are key regulators of Mg^{2+} homeostasis: mutations of TRPM6 cause familial hypomagnesemia and secondary hypocalcemia (20, 21); whereas targeted gene deletion of TRPM7 in the DT40 B cell line produced intracellular Mg^{2+} deficiency and growth arrest (7, 22). Consistent with its role in Mg^{2+} and Ca^{2+} homeostasis, TRPM6 is abundantly expressed in the intestine and the kidney (8, 20, 21, 23), whereas TRPM7 is ubiquitously expressed, with highest expression in the kidney and heart (5, 6). In addition to these channels' regulation of Mg^{2+} homeostasis, several studies have suggested multiple cellular and physiology functions for TRPM7, including anoxic neuronal death (24), cell adhesion and actomyosin contractility (25, 26), and skeletogenesis (27). Although the mechanisms by which TRPM6 and TRPM7 exert their physiological and/or pathological functions are not yet completely understood, it is clear that permeation of Ca^{2+} and Mg^{2+} contributes substantially to the known functions of these channels (7, 20–22, 24, 25, 27). Moreover, a recent study demonstrated that the sensitivity of TRPM7 to external pH may contribute to controlling neurotransmitter release (28). Therefore, it is essential to understand the molecular mechanisms underlying the Ca^{2+} and Mg^{2+} permeability of TRPM6 and TRPM7, as well as their sensitivities to changes in pH.

The aim of the present study was to identify the amino acid residues that determine Mg^{2+} and Ca^{2+} permeation of TRPM6 and TRPM7. We previously demonstrated that external protons significantly enhance TRPM6 and TRPM7 inward currents (11, 19) by decreasing the divalent affinity to the channels. Our results suggested that protons compete with divalents for binding site(s) within the channels' pore. In the present study, we systematically mutated negatively charged amino acid residues within the putative pore-forming region of TRPM7; and identified Glu^{1047} and Glu^{1052} of TRPM7 as the key residues that confer divalent selectivity and the sensitivity of the channel to pH. Moreover, we demonstrated that mutations of the equivalent positions (Glu^{1024} and Glu^{1029}) in TRPM6 produced identical changes, indicating that these two glutamate residues constitute the molecular basis of these channels' Mg^{2+} and Ca^{2+} permeability as well as their pH sensitivity. The above findings are critical to understanding the physiological/pathological functions of TRPM6 and TRPM7, and provide molecular insight of the pore architecture of these channels.

EXPERIMENTAL PROCEDURES

Molecular Biology

TRPM6 construct was kindly provided by Dr. Joost G. J. Hoenderop. TRPM7 was previously cloned from mouse (6). Amino acid substitutions to the pores of TRPM6 and TRPM7 were made using the QuikChange Site-directed Mutagenesis Kit (Stratagene) following the manufacturer's instructions. The primers are shown in supplemental materials Table S1.

Functional Expression of TRPM6, TRPM7, and the Mutants

CHOK1 cells were grown in Dulbecco's modified Eagle's medium/Ham's F-12 medium supplemented with 10% fetal bovine serum, 100 units/ml penicillin, and 100 mg/ml streptomycin at 37 °C in a humidity-controlled incubator with 5% CO_2. Cells were transiently transfected with wild-type (WT)[5] TRPM6, TRPM7, and the mutants of TRPM6 and TRPM7 as previously described (6). TRPM7 and its mutants were co-transfected with a green fluorescent protein-containing pTracerCMV2 vector. Electrophysiological recordings were conducted between 36 and 48 h after transfection. Successfully transfected cells were

[5]The abbreviations used are: WT, wild type; VGCC, voltage-gated Ca^{2+} channels; DVF, divalent-free solution; NMDG, *N*-methyl-D-glucamine; MES, 4-morpholineethanesulfonic acid.

identified by their green fluorescence when illuminated at 480 nm. All patch-clamp experiments were performed at room temperature (20–25 °C).

Electrophysiology

Whole cell currents were recorded using an Axopatch 200B amplifier. Data were digitized at 10 or 20 kHz, and digitally filtered off-line at 1 kHz. Patch electrodes were pulled from borosilicate glass and fire-polished to a resistance of ~3 MΩ when filled with internal solutions. Series resistance (R_s) was compensated up to 90% to reduce series resistance errors to <5 mV. Cells in which R_s was >10 MΩ were discarded (29).

For whole cell current recordings, voltage stimuli lasting 250 ms were delivered at 1–5-s intervals, with either voltage ramps or voltage steps ranging from −120 to +100 mV. Unless otherwise stated, following break-in, 3–5 min were allowed to pass to let currents develop to reach a steady-state. A fast perfusion system was used to exchange extracellular solutions, with complete solution exchange achieved in ~1–3 s (19).

The internal pipette solution (P1) for whole cell current recordings contained (in mM) 145 cesium methanesulfonate, 8 NaCl, 10 EGTA, and 10 HEPES, with pH adjusted to 7.2 with CsOH. In some experiments (supplementary materials Fig. S1), Mg^{2+} was added to the pipette solution and the free Mg^{2+} concentration was titrated to 3 mM (calculated with the MaxChelator software, available at stanford.edu/~cpatton/webmaxcS.htm). In experiments designed to diminish outward currents, pipette solution (P2) contained (mM): NMDG 120, glutamic acid 108, HEPES 10, EGTA 10, CsCl 10, and pH was adjusted to 7.2 with NMDG.

The standard extracellular Tyrode's solution contained (mM): 140 NaCl, 5 KCl, 2 $CaCl_2$, 20 HEPES, and 10 glucose, pH adjusted to 7.4 (NaOH). External solutions at various acidic pH were prepared as previously reported (19, 30–32). In brief, HEPES (20 mM) was used in the solutions at pH 7.0 and 7.4, and was replaced by 10 mM HEPES and 10 mM MES for the solutions at pH ≤6. Divalent-free solution (DVF) contained (mM) 145 NaCl, 20 HEPES, 5 EGTA, 2 EDTA, and 10 glucose, with estimated free [Ca^{2+}] <1 nM and free [Mg^{2+}] ≈10 nM at pH 7.4 (calculated with the MaxChelator software). Appropriate Ca^{2+} or Mg^{2+} was added to the DVF at pH 7.4 to prepare solutions containing ≤10 μM Mg^{2+} or Ca^{2+} (Fig. 5). Solutions containing 0.1, 0.2, 0.5, 1, 2, and 10 mM Mg^{2+} or Ca^{2+} were prepared by omitting EDTA and EGTA in the DVF solution, and by adding the appropriate concentrations of Mg^{2+} or Ca^{2+}, with reductions in Na^+ concentration when necessary to maintain constant osmolarity. Isotonic Ca^{2+} or Mg^{2+} solution contained 120 mM Ca^{2+} or Mg^{2+}, 10 mM HEPES, 10 mM glucose, with pH adjusted to pH 7.4. Different cation solutions (Fig. 7) at 30 mM contained (in mM): 30 divalents or monovalents, 20 HEPES, 100 NMDG-Cl, 10 glucose (pH 7.4). Zn^{2+} solution was prepared at 10 mM due to the low solubility (11). All chemical reagents were purchased from Sigma.

Ion permeation ratios are typically calculated from reversal potentials (E_{rev}) using Nernst and Goldman-Hodgkin-Katz equations based on the assumption that ions permeate independently and that the electric field in the membrane is constant (33). For TRPM7 channels, however, because the monovalent and divalent cations do not permeate the channels independently (7), it is not adequate to use the Goldman-Hodgkin-Katz equation to estimate the relative permeability (7, 8, 12). Thus, the relative permeability was estimated from the inward current amplitude as previously reported (8, 12).

Data Analysis

Pooled data are presented as mean ± S.E. Dose-response curves were fitted by an equation of the form: $E = E_{max}\{1/[1 + (EC_{50}/C)^n]\}$, where E is the effect at concentration C, E_{max} is the maximal effect, EC_{50} is the concentration for half-maximal effect, and n is the Hill

coefficient (34). EC_{50} is replaced by IC_{50} if the effect is an inhibitory effect. Voltage-dependent effects of Ca^{2+} and Mg^{2+} on TRPM7 and the mutants were analyzed by fitting the I/I_0 ratio curves to the Boltzmann functions: $I/I_0 = 1/(1 + \exp[V_{0.5} - V]/k)$ is for the voltage-dependent block, and $I/I_0 = 1/(1 + \exp[V - V_{0.5}]/k)$ is for the voltage-dependent relief of block; where I_0 is the current before and I is the current after application of Mg^{2+} or Ca^{2+}, V is the membrane potential, $V_{0.5}$ is the membrane potential at which the current is blocked by 50%, and k is a slope factor representing the voltage dependence of block (35). The slope factor k is $k = RT/z\delta F$, where z is the valence of blocker and δ is the fraction of the membrane electrical field. Statistical comparisons were made using two-way analysis of variance and two-tailed t test with Bonferroni correction; $p < 0.05$ indicated statistical significance.

RESULTS

E1047Q and E1052Q Substitutions within TRPM7 Pore Alters Its I–V Relationship

When heterologously expressed, TRPM7 constitutes a channel that is characterized by extremely small inward and large outward currents. External divalent cations such as Mg^{2+} and Ca^{2+} are permeable to TRPM7 and at the same time block monovalent cations permeating through the pore of the channel. We have previously shown that external protons substantially potentiate TRPM7 inward currents, which may occur through competition of protons with divalent cations for binding sites in the pore of the channel (19). To identify potential binding sites for Mg^{2+}, Ca^{2+}, as well as for protons, we systematically exchanged negatively charged residues within the TRPM7 putative pore region with uncharged residues found at equivalent positions in other TRPM family members (Fig. 1). As the increase in inward current induced by pH for TRPM6 is smaller than that observed for TRPM7 (11, 19), we also investigated the contribution of His^{1039} to the pH sensitivity of TRPM7 because His^{1039} is replaced by Glu in TRPM6. Therefore, we additionally mutated His^{1039} to H1039E and H1039M, as TRPM1 and TRPM3 have a Met residue at the equivalent positions, respectively. Within the S5–S6 linker of TRPM7, eight residues were singly or doubly mutated (Fig. 1). The resulting TRPM7 mutants were transiently transfected into CHO-K1 cells and their currents examined for sensitivity to pH and permeability to Mg^{2+} and Ca^{2+}. Because the endogenous TRPM7-like MIC/MagNuM current is extremely small in CHO-K1 cells (6), the elicited currents obtained upon transfection of the TRPM7 mutants predominantly reflect conductances originating from the expressed TRPM7 pore mutants.

Fig. 2 shows currents recorded from various TRPM7 mutants. The current-voltage (I–V) relationships of the mutants D1035N, D1054A, H1039E, and H1039E were similar to that of WT TRPM7. It was surprising that D1054A did not produce a significant change, as this aspartic acid residue is conserved among all TRPM channels. By contrast, the I–V relationships of E1047Q and E1052Q were significantly different from that of WT TRPM7. The inward current of E1052Q was substantially larger than that of WT TRPM7, whereas its outward current was similar to WT TRPM7. E1047Q demonstrated a double rectification I–V profile, with increased inward current and decreased outward current compared with WT TRPM7. The normalized I–V curves of D1035N, D1054A, H1039E, and H1039M were superimposable with that of WT TRPM7, whereas the I–V curves of E1047Q and E1052Q were markedly different from that of WT TRPM7 (Fig. 2*H*). The average inward and outward current amplitudes obtained for the TRPM7 pore mutants are summarized in Fig. 3*A*. The ratios of inward currents measured at −120 mV to the outward currents measured at +100 mV of E1047Q and E1052Q were 12- and 8-fold larger than that of WT TRPM7 (Fig. 3*B*), respectively; indicating that blockade of monovalent inward current by divalent cations was reduced in E1047Q and E1052Q compared with WT TRPM7. The significant changes in current-voltage profiles in E1047Q and E1052Q indicate that E1047 and E1052 are residues critical to TRPM7 channel function.

In the mutants in which the negatively charged Glu was replaced by positively charged Lys at Glu^{1047} and Glu^{1052} positions (E1047K and E1052K), a majority of cells transfected with E1047K and E1052K did not produce measurable currents (data not shown). We were unable to detect expression of the E1052K mutant, suggesting that the amino acid substitution may have affected the overall stability of the protein. However, expression of E1047K was confirmed by Western blot analysis (data not shown), suggesting that either the E1047K mutant is completely inactive or unable to traffic to the cell membrane, thereby indicating that Glu^{1047} is essential for TRPM7 channel function.

Changes in pH Sensitivity in TRPM7 Mutants

For the WT TRPM7 channels, acidification of extracellular bath solution increased the inward current by about 12-fold when the pH was lowered from pH 7.4 to 4.0 (Fig. 4, *A_1–A_2*). Similar increases in the inward currents were observed in the H1049E and H1039M mutants (Fig. 4, *F_1–F_2* and *G_1–G_2*). The magnitude of the increase in inward current by acidic external bath solutions was considerably smaller for mutants E1052Q, D1035N, and D1054A. However, no significant difference in $pH_{1/2}$ (Fig. 4, *A_3* and *C_3–G_3*) was obtained for D1035N, H1039E, H1039M, D1054A, and E1052Q mutants compared with WT TRPM7. Surprisingly, unlike WT TRPM7 and the other pore mutants, external protons inhibited E1047Q currents in a concentration-dependent manner (Fig. 4*B_1*). The maximal inhibition was about 30%, with an IC_{50} of pH 5.4. This unexpected result indicates that Glu^{1047} substantially contributes to proton binding, and is therefore likely to be the major binding site for divalent cations.

Mutations at Glu^{1047} and Glu^{1052} Change the Affinity of TRPM7 for Divalent Cations

We next examined whether the divalent affinity for TRPM7 was changed when negatively charged residues in the putative pore region of the channels were mutated to uncharged amino acids. The inward current of WT TRPM7 carried by monovalent cations can be blocked by micromolar concentrations of Ca^{2+} or Mg^{2+} (Fig. 5, *A* and *D*), with the IC_{50} values of 4.1 ± 0.2 (Fig. 5*G*) and 3.6 ± 0.4 μM (Fig. 5*H*), respectively. Monovalent currents produced by D1035N and D1054A were similarly blocked by Ca^{2+} and Mg^{2+}, with the IC_{50} values nearly identical to those of WT TRPM7 (Fig. 5, *G–H*). The dose-response curves (Fig. 5, *G–H*) of D1035N and D1054A were superimposable with those of WT TRPM7. Unlike D1035N and D1054A, higher concentrations of Ca^{2+} and Mg^{2+} were required to block monovalent currents produced by E1047Q and E1052Q (Fig. 5, *B*, *E*, *C*, and *F*). The dose-response curves for E1047Q and E1052Q were markedly shifted to the right, with IC_{50} values increased by 50- (E1052Q) to 140-fold (E1047Q) compared with WT TRPM7. These results indicate that the affinities of Ca^{2+} and Mg^{2+} for the TRPM7 mutants E1047Q and E1052Q were significantly decreased, indicating that Glu^{1047} and Glu^{1052} residues are critical sites for Ca^{2+} and Mg^{2+} binding.

We also tested the effects of Ca^{2+} and Mg^{2+} on the monovalent currents of H1039E and H1039M. The IC_{50} values of the Ca^{2+} block were 2.3 ± 0.4 μM (n =6, n_H = 1.0) and 2.6 ± 0.5 μM (n = 6, n_H = 1.0) for H1039M and H1039E, respectively; whereas the IC_{50} values for the Mg^{2+} block were 3.4 ± 0.6 μM (n =6, n_H = 0.7) and 3.5 ± 0.4 μM (n = 6, n_H = 0.8) for H1039M and H1039E, respectively. No statistical significant difference in IC_{50} values of Ca^{2+} and Mg^{2+} block of H1039M and H1039E was observed as compared with WT TRPM7, indicating that the His^{1039} residue is not essential for Ca^{2+} or Mg^{2+} binding to TRPM7.

Changes in Voltage-dependent Block by Mg^{2+} and Ca^{2+} in Mutants E1047Q and E1052Q

It has been shown that divalent cations block monovalent currents of MIC/MagNuM and TRPM7 in a voltage-dependent manner (35, 36). We therefore compared the voltage-

dependent effects of Ca^{2+} and Mg^{2+} on monovalent currents of WT TRPM7, E1047Q, and E1052Q. As shown in Fig. 6, WT TRPM7 monovalent current was the most potently blocked at −40 mV (Fig. 6, *A* and *D*) with an IC_{50} of 1.0 μM (Fig. 6*A*), whereas the IC_{50} values at −120, −80, +40, and +80 mV were 3.6, 1.8, 51.5, and 1573 μM, respectively. The smaller inhibition or the relief of Mg^{2+} inhibition on TRPM7 at hyperpolarized potentials (Fig. 6, *A*, *D*, and *G*) may suggest "punch-through" of Mg^{2+} to the inside, consistent with the notion that Mg^{2+} is a permeant blocker for TRPM7 (35). The best fit of Mg^{2+} block with a Boltzmann equation estimated the equivalent electrical distance across the δ membrane from the extracellular side (δ_{out}) to be 0.84 for Mg^{2+} (Fig. 6*G* and supplementary materials Table S2), indicating that extracellular Mg^{2+} binds to TRPM7 at a site of 84% of the membrane electrical field. The Boltzmann equation fit to the relief of the Mg^{2+} block yielded the fractional electrical distance δ from the intracellular side (δ_{in}) to be 0.25. The fact that our calculated δ_{out} and δ_{in} values do not add up to exactly 1.0 could be explained in several ways, including: 1) there may be multiple Mg^{2+} ions binding to the pore (33); 2) the blocking ion Mg^{2+} may compete with permeating ion Na^{+}; 3) there may be conformational changes of the channel caused by binding of the blocking ions; and 4) there may be coupled movement of the blocking ion and permeant ion through the ion channels (33, 35, 37).

Similar to WT TRPM7, E1052Q also exhibited a voltage-dependent block by Mg^{2+} (Fig. 6, *C*, *F*, and *I*), albeit the voltage dependence was less dramatic compared with that of WT TRPM7, as evidenced by the shallower slope of I/I_0 curves (Fig. 6*I*). The best fit of the voltage-dependent block with a Boltzmann function yielded the equivalent electrical distance across the membrane δ_{out} of 0.52 (Fig. 6*I*), indicating that a Mg^{2+} binding site in E1052Q is located close to the outside surface of the membrane. The Boltzmann equation fit to the relief of the voltage-dependent block on E1052Q yielded δ_{in} of 0.43 (supplementary materials Table S2). In contrast to WT TRPM7 and E1052Q, the Mg^{2+} block on E1047Q was barely relieved at hyperpolarizing potentials as evidenced by the flat I/I_0 curves at negative potentials (Fig. 6*H*) and the virtually identical IC_{50} values at −120, −80, and −40 mV (Fig. 6, *B* and *E*), indicating that the blocking ion Mg^{2+} encounters a large energy barrier and cannot penetrate all the way through the pore (38). Thus, E1047Q may not be able to support measurable Mg^{2+} currents. The best fit of the voltage-dependent block of Mg^{2+} on E1047Q with the Boltzmann equation estimated the fractional electrical distance across the membrane δ_{out} of 0.36, suggesting that Mg^{2+} binds to a shallow site (Fig. 6) with low affinity (Figs. 5 and 6) in E1047Q.

The voltage- and concentration-dependent effects of Ca^{2+} on TRPM7, E1047Q, and E1052Q were similar to the effects of Mg^{2+}. The IC_{50} values of the Ca^{2+} block on TRPM7 monovalent currents were 4.1 ± 0.2 μM at −120 mV, 1.9 ± 0.4 μM at −80 mV, 0.9 ± 0.2 μM at −40 mV, 93.9 ± 12.1 μM at +40 mV, and 1.3 ± 0.2 mM at +80 mV (n = 6 at each concentration), respectively; the IC_{50} values of Ca^{2+} block on monovalent currents of E1047Q were 593.6 ± 69.9 μM at −120 mV, 578.1 ±63.4 μM at −80 mV, 561.8 ± 73.6 μM at −40 mV, 5.9 ± 0.6 mM at +40 mV, and 7.6 ± 0.7 mM at +80 mV (n = 6), respectively; and Ca^{2+} block on monovalent currents of E1052Q were 202.2 ± 14.3 μM at −120 mV, 132.5 ± 14.7 μM at −80 mV, 67.2 ± 8.2 μM at −40 mV, 312.1 ± 25.7 μM at +40 mV, and 1.3 ±0.2 mM at +80 mV, respectively. The values of the fractional electrical distance δ_{out} calculated based on $k = RT/z\delta F$ were 0.81, 0.33, and 0.56 for TRPM7, E1047Q, and E1052Q, respectively (supplemental materials Table S2).

We further examined if E1047Q and E1052Q affected the ability of internal Mg^{2+} to block TRPM7 currents. We found that mutations at Glu^{1047} and Glu^{1052} did not change internal Mg^{2+} inhibition on TRPM7 currents (supplemental materials Fig. 1), indicating that these residues are not the binding sites for internal Mg^{2+}. This is consistent with the notion that internal Mg^{2+} is not accessible to the channel pore, because internal Mg^{2+} blocks TRPM7 in

a voltage-independent manner (15). A model proposed in a recent study also suggests that the internal Mg^{2+} binding sites are located in the C terminus of TRPM7: one site is located in the kinase domain and the second site is located upstream of the kinase domain (39).

Changes in Relative Permeability by Mutations at Glu^{1047} and Glu^{1052}

The larger inward currents observed in E1052Q and E1047Q mutants (Fig. 2) and their reduced apparent affinity for Ca^{2+} and Mg^{2+} (Fig. 5 and 6) prompted us to determine whether the relative permeability of these mutants to Ca^{2+}, Mg^{2+}, and other divalent cations were altered as well (11, 12). We assessed the relative permeability by evaluating changes in the current amplitude as previously reported (7, 8, 12). Divalent cations at 30 mM were used to achieve larger inward currents so that more precise measurements of the relative permeability could be obtained. Zn^{2+} was prepared at 10 mM due to its low solubility at pH 7.4 (11). Fig. 7, *A*–*E*, shows the ratios of current amplitude of the indicated cations normalized to the current amplitude measured in the solution containing 30 mM Ca^{2+}. The mutants D1035N and D1054A exhibited substantial permeation to different divalents with a relative permeability to different cations similar to that observed for WT TRPM7 (Fig. 7, *A*, *B*, and *E*). In contrast with D1035N and D1054A, E1052Q exhibited a decreased divalent permeability, as was evident from the ratio of I_{Tyrode}/I_{Ca} being substantially larger than that of I_{Ni}/I_{Ca} (Fig. 7*D*). In addition, Ba^{2+} permeation through E1052Q appeared smaller than that of WT TRPM7, D1035N, and D1054A (Fig. 7, *A*–*D*). Nevertheless, all the tested divalents permeated through E1052Q. Intriguingly, E1047Q exhibited very little permeation to the divalents such that Mg^{2+}, Ca^{2+}, and Zn^{2+} currents were barely detectable (Fig. 7*C*). By contrast, the ratio of I_{Tyrode}/I_{Ca} for E1047Q was significantly larger than that for WT TRPM7 and other mutants, indicating that currents through E1047Q in Tyrode solutions were mainly carried by monovalent cations. Fig. 7*F* shows the normalized Mg^{2+} and Ca^{2+} currents *versus* the current amplitude obtained in Tyrode solution. In E1047Q, the current amplitude of Mg^{2+} and Ca^{2+} was only 1.1 and 2.3% of that observed in WT TRPM7, respectively. In E1052Q, the current amplitude carried by Mg^{2+} and Ca^{2+} was 24.3 and 24.1% of that observed in WT TRPM7, respectively. These results strongly suggest that Glu^{1047} is the dominant residue that confers Ca^{2+} and Mg^{2+} permeability to TRPM7. In contrast to the changes to divalent permeability, the sequence for monovalent permeability ($K^+ > Cs^+ > Na^+$) (Fig. 7, *A*–*E*) was not changed in all the mutants tested compared with WT TRPM7.

Mutation of Glu^{1047} Diminishes Ca^{2+} Permeation and Largely Eliminates Mg^{2+} Permeation

We further studied the Ca^{2+} and Mg^{2+} permeation properties of E1047Q and E1052Q using isotonic Ca^{2+} and Mg^{2+} solutions (120 mM Ca^{2+} or Mg^{2+}). Currents were recorded using a P2 pipette solution to minimize outward currents. In WT TRPM7, the inward current amplitude in isotonic Ca^{2+} and Mg^{2+} solutions was similar to that in Tyrode solution or in 2 mM Ca^{2+}, 150 mM monovalent solutions (Fig. 8, *A*, *D*, and *G*). Changes in reversal potentials of TRPM7 in isotonic Ca^{2+} and Mg^{2+} solutions were also similar to those in 2 mM Ca^{2+}/monovalent solutions (Fig. 8*J*). In clear contrast to WT TRPM7, the inward current amplitude of E1047Q in isotonic Ca^{2+} and Mg^{2+} solutions was significantly smaller than those in 2 mM Ca^{2+} Tyrode solution (Fig. 8, *B* and *E*). There was almost no Mg^{2+} conductance in isotonic Mg^{2+} solution, as shown in Fig. 8, *B* and *E*. The average current amplitude shown in Fig. 8*H* also indicates that the Ca^{2+} current was significantly reduced, whereas the Mg^{2+} current was almost undetectable in the E1047Q mutant. The isotonic Mg^{2+} and Ca^{2+} current amplitude of E1047Q (Fig. 8*H*) was 2.1 and 6.0% of the current amplitude of WT TRPM7 (Fig. 8*G*), respectively. Consistent with the small conductances in the isotonic solutions, the reversal potentials of E1047Q in isotonic Ca^{2+} and Mg^{2+} solutions were much more negative than that in Tyrode solution (Fig. 8, *B* and *K*). Unlike E1047Q, E1052Q exhibited substantial inward Ca^{2+} and Mg^{2+} currents (Fig. 8, *C*, *F*, and *I*), albeit the

current amplitude was smaller compared with that of WT TRPM7. Changes in reversal potentials under the indicated conditions in reference to the value obtained in Tyrode solution were smaller than those of WT TRPM7 (Fig. 8*J*), but much larger than those of E1047Q (Fig. 8*L*). Based on the above results, we conclude that E1047Q and E1052Q are critical for Mg^{2+} and Ca^{2+} permeation through TRPM7.

Mutations of Glu^{1024} and Glu^{1029} Changes Divalent Permeability and pH Sensitivity of TRPM6

The above results strongly suggest that Glu^{1047} and Glu^{1052} are key amino acid residues that confer Mg^{2+} and Ca^{2+} selectivity to TRPM7. To further confirm the importance of Glu^{1047} and Glu^{1052} in Ca^{2+} and Mg^{2+} permeation, we generated mutants E1024Q and E1029Q in TRPM6 at the equivalent positions for Glu^{1047} and Glu^{1052} in TRPM7, respectively. As shown in Fig. 9, *A–C*, TRPM6 mutants E1024Q and E1029Q exhibited significant changes in their I–V relationship compared with WT TRPM6. The normalized I–V curves (Fig. 9*D*) show that the ratios of inward currents at −120 mV *versus* outward currents at +100 mV of E1024Q (0.7) and E1029Q (0.3) were 14- and 6-fold larger than that of WT TRPM6 (0.05). The I–V relationships for E1029Q and E1024Q in TRPM6 were similar to the TRPM7 mutants E1052Q and E1047Q (Fig. 2).

We next determined whether the binding affinity of the TRPM6 pore mutants for divalents was changed. Similar to what we observed for E1047Q and E1052Q, the affinity of Ca^{2+} and Mg^{2+} was significantly decreased in TRPM6 mutants E1024Q and E1029Q (Fig. 9, *E* and *F*). The IC_{50} values of Ca^{2+} block of monovalent currents were 4.6 μM for TRPM6, 153.5 μM for E1024Q, and 50.5 μM for E1029Q, respectively; and IC_{50} values of Mg^{2+} block on monovalent currents were 3.4 ± 0.3 μM for TRPM6, 237.2 μM for E1024Q, and 149.2 μM for E1029Q, respectively. Consistent with the decreased affinity for Ca^{2+} and Mg^{2+}, the permeation of Ca^{2+} and Mg^{2+} was also largely decreased. As shown in Fig. 9*G*, the inward current amplitude of the WT TRPM6 obtained in isotonic Ca^{2+} and Mg^{2+} solutions were similar to the current amplitude in Tyrode solution. By contrast, Ca^{2+} currents of E1024Q and E1029Q obtained in the isotonic solutions were significantly smaller than those obtained from WT TRPM6 (Fig. 9, *G–I*). Moreover, there was almost no Mg^{2+} permeation through E1024Q (Fig. 9, *H* and *J*). These results indicate that similar to Glu^{1047} and Glu^{1052} in TRPM7, Glu^{1024} and Glu^{1029} residues are essential for the Mg^{2+} and Ca^{2+} permeability of TRPM6.

As TRPM6 is sensitive to acidic pH (11), we next tested if the pH sensitivity was changed in mutants E1024Q and E1029Q. As shown in Fig. 10, external protons enhanced inward currents of E1029Q (Fig. 10, *C*, *F*, and *I*). The degree of increase in E1029Q inward currents was smaller than the increase in TRPM6 inward current induced by low pH, but similar to the changes in E1052Q (Fig. 4, C_1–C_3). In contrast to E1029Q, E1024Q was blocked by acidic external solutions by 42% at pH 3.0 (Fig. 10, *B*, *E*, and *H*) with an IC_{50} of pH 5.0. Thus, similar to what we found for residues Glu^{1047} and Glu^{1052} in TRPM7, TRPM6 residues Glu^{1024} and Glu^{1029} are critical determinants of the sensitivity of the channel to external pH.

Double Mutant E1047Q/E1052Q Exhibits Similar Properties to Those of E1047Q

Because mutation of Glu^{1047} in TRPM7 produced dramatic changes in TRPM7 channel properties, and mutation of Glu^{1052} also generated substantial changes in Ca^{2+} and Mg^{2+} permeability as well as pH sensitivity, this prompted us to ask how mutation of both sites (E1047Q/E1052Q) would affect TRPM7 channel properties. Fig. 11*A* shows that the E1047Q/E1052Q current elicited by a ramp protocol exhibited a double rectifying I–V relation similar to that of E1047Q (Fig. 2, *E* and *H*). Like E1047Q, the inward currents in

isotonic Ca^{2+} or Mg^{2+} solutions (120 mM) were almost undetectable (Fig. 11, *B–D*), and the reversal potentials of E1047Q/E1052Q in isotonic Ca^{2+} and Mg^{2+} solutions were almost identical to those in NMDG solutions (Fig. 11*B*), suggesting a largely reduced permeability to Ca^{2+} and Mg^{2+}. Consistent with this notion, Mg^{2+} affinity for E1047Q/E1052Q was significantly smaller than that of WT TRPM7. At −120 mV, IC_{50} of the Mg^{2+} block on the monovalent currents of the double mutant was 132.7 μM (Fig. 11*E*). The voltage-dependent effect of Mg^{2+} on the E1047Q/E1052Q monovalent currents (Fig. 11, *E* and *F*) was also similar to that of E1047Q. IC_{50} values of Mg^{2+} block at −120, −80, and −40 mV were almost identical, indicating that there was no relief of Mg^{2+} block at hyperpolarizing potentials. Consistent with this notion, the current ratio (I/I_0) and voltage relation (Fig. 11*F*) shows a virtually flat line at hyperpolarizing voltages, further suggesting that the punch-through mechanism of Mg^{2+} permeation had been disabled in E1047Q/E1052Q. The best fit of a Boltzmann equation to I/I_0 curves produced a slope factor k of 29 mV, generating the estimated distance of the electrical field δ_{out} = 0.44 from the outside surface of the membrane. Similar to the effects of Mg^{2+}, the IC_{50} values of Ca^{2+} block on E1047Q/E1052Q were 164.6 ± 20.7 μM at −120 mV, 170.3 ± 24.6 μM at −80 mV, 166.9 ± 26.7 μM at −40 mV, 723.1 ± 89.4 μM at +40 mV, and 2.4 ±0.3 mM at +80 mV, respectively (n = 5). The lack of voltage-dependent relief of Ca^{2+} block at hyper-polarized potentials further suggests the diminished divalent permeation through E1047Q/E1052Q. The above similar properties between E1047Q/E1052Q (Fig. 11) and E1047Q (Fig. 6) strongly suggest that, like the E1047Q mutation, double mutation of Glu^{1047} and Glu^{1052} largely eliminated a high-affinity divalent binding site that is present in the deep pore of WT TRPM7.

Unlike E1047Q currents, which were slightly inhibited by acidic external solutions (Fig. 4, B_1–B_3), the inward currents of the double mutant E1047Q/E1052Q were increased to a small degree by high concentrations of external protons (Fig. 11, *E* and *F*). This potentiation of inward currents of E1047Q/E1052Q by low pH was similar to that of E1052Q, although the degree of increase was much smaller than that in E1052Q. These results provide further evidence that residues Glu^{1047} and Glu^{1052} are indeed important in determining divalent permeability and pH sensitivity of TRPM7.

DISCUSSION

In the present study, we demonstrate that mutation of Glu^{1052} decreases its Ca^{2+} and Mg^{2+} permeability; whereas mutation of Glu^{1047} largely eliminates Ca^{2+} and Mg^{2+} permeability and converts TRPM7 into a monovalent selective cation channel. In addition, external protons, which significantly increase TRPM7 inward currents, fail to enhance the inward currents of E1047Q. Furthermore, mutations at the equivalent sites in TRPM6, E1024Q and E1029Q, produce similar phenotypic changes to those observed in E1047Q and E1052Q. These results indicate that Glu^{1047}/Glu^{1052} in TRPM7 and Glu^{1024}/Glu^{1029} in TRPM6 are essential for the Mg^{2+} and Ca^{2+} permeability and pH sensitivity of these channels.

Glu^{1047} and Glu^{1052} Are Key Amino Acid Residues That Determine Divalent Permeability and pH Sensitivity

A unique feature of TRPM6 and TRPM7 is their permeation of Ca^{2+} and Mg^{2+}, which confers their physiological and pathological functions (7, 20–22, 24). Our previous study (11) suggested that negatively charged residues within the channel pore contribute to divalent permeability. In the present study, by systematically substituting the negatively charged residues in the putative pore region of TRPM7 with uncharged residues, we identified Glu^{1047} and Glu^{1052} as the key residues for Ca^{2+}/Mg^{2+} permeability and pH sensitivity. This conclusion is supported by the fact that mutations at the equivalent positions in TRPM6 (Glu^{1024} and Glu^{1029}) generated similar changes in divalent permeability and pH sensitivity. It is remarkable that neutralization of a single amino acid

residue, E1047Q (or E1024Q), largely eliminated divalent permeation, converting the divalent selective TRPM7 (or TRPM6) to a virtually monovalent selective channel, and at the same time abolished external pH sensitivity. The feature that the divalent selectivity and pH sensitivity are conferred by the same residue in TRPM6 and TRPM7 is unique among TRP channels. It is known that TRPV5 (or TRPV6) is highly Ca^{2+} selective (34, 40) and also sensitive to external pH (41, 42). However, the pH sensitivity mediated by Glu^{522} in TRPV5 is independent of its Ca^{2+} selectivity determined by Asp^{542} (42, 43). TRPV1 channel activity is regulated by acidic pH through Glu^{600} and Glu^{648} residues (30), whereas its divalent permeability appears to be mediated by Asp^{646} (44). External low pH activates TRPV4 (45), yet it is unknown whether this pH sensitivity of the channel is correlated with its Ca^{2+} permeation determined by Asp^{672} and Asp^{682} residues in the pore (46). The monovalent selective channel TRPM5 is also inhibited by protons (47). Nonetheless, the molecular mechanism of pH sensitivity and divalent permeability of TRPM7/TRPM6 resembles to some extent the properties of the voltage-gated Ca^{2+} channels (VGCCs). It has been demonstrated that protons block VGCCs by binding to the Ca^{2+} binding sites, Glu residues, in the pore-forming region (48, 49). Mutation of Glu by Gln replacement in repeats *I* or *III* abolished the high-conductance state of VGCCs, as if the titration site had become permanently protonated (48). Like VGCCs, mutation of Glu^{1047} in TRPM7 (or Glu^{1024} in TRPM6) increased inward monovalent currents, resembling the effect produced when the external bath solution is acidified on WT TRPM7 (or TRPM6) currents (11). Furthermore, TRPM6 and TRPM7 lose their high affinity binding sites when Glu^{1024}/Glu^{1047} and Glu^{1029}/Glu^{1052} are replaced by Gln, similar to the loss of high affinity binding sites for divalent cations in VGCCs when the pore Glu residues are mutated (38).

It is noticeable that both E1047Q and E1052Q produced substantial changes in channel properties compared with WT TRPM7, although the changes such as I–V relation, decreased affinity to Ca^{2+} and Mg^{2+}, and diminished divalent permeation in E1052Q are less dramatic than those observed in E1047Q. The double mutant E1047Q/E1052Q exhibited similar properties to those of E1047Q, suggesting that although both Glu^{1047} and Glu^{1052} are essential, Glu^{1047} dominates in determining divalent permeability and pH sensitivity. Using the Eyring rate model (35), Kerschbaum and colleagues predicted a high affinity site for binding Mg^{2+} within the electric field and two low affinity sites for MIC/TRPM7 channel. In agreement with this notion, our data indicate that Glu^{1047} and Glu^{1052} compose a high affinity binding site. Mutation of either or both of these residues disrupts the high affinity site (Figs. 5 and 6). As we used single Boltzmann functions for data analysis, our data suggest that there is one low affinity site after mutation of the high affinity site Glu^{1047}/Glu^{1052}.

Analysis of the voltage-dependent effects of Mg^{2+}/Ca^{2+} suggests that the high affinity site is located at about 84% of the electrical distance of membrane, similar to the value estimated by Kerschbaum and colleagues (35) for the MIC/TRPM7 channel. The fractional electrical distance from the outside surface of the membrane δ_{out} estimated based on the Mg^{2+} block changes from 0.84 in WT TRPM7 (Fig. 6) to 0.36 in E1047Q, and 0.52 in E1052Q. In the double mutant, the δ_{out} (0.44) is close but not identical to that of E1047Q or E1052Q, suggesting that a low affinity site is located between δ_{out} of 0.36 and 0.52. The differences in δ_{out} for the potential low affinity site may be a reflection of experimental variations, or may represent reorganization of the pore structure after mutating of Glu^{1047}, Glu^{1052}, and Glu^{1047}/Glu^{1052}. In addition, we used the simplest model for data analysis, which assumes one permeant ion occupies a binding site in the channel pore (50). This may also contribute to the variances in estimated δ_{out} for the low affinity site. Nonetheless, our data indicate that a low affinity site is located close to the outer surface of the cell membrane. Taken together, our results suggest that a high affinity binding site comprising Glu^{1047} and Glu^{1052} is

located deep within the pore (82 to 84%), whereas a low affinity binding site is shallower, within 36 –52% of the electrical distance of membrane.

Selectivity Filter of TRPM6 and TRPM7

TRP channels vary from each other by their gating mechanisms and permeability profiles. TRPV5 and TRPV6 have the highest Ca^{2+} selectivity (51), whereas TRPM4 and TRPM5 are monovalent selective and impermeable to divalent cations (52–55). Similar to VGCCs, the Ca^{2+} selectivity of TRPV5/TRPV6 is determined by a single pore residue, Asp^{542} (43). The acidic residues in the putative pore of TRPV1 (Asp^{646}) (44) and TRPV4 (Asp^{682}) (46) are also involved in divalent permeability. The pore structure of TRPM channels is less well defined (51). A recent study by Nilius and colleagues (56) revealed that an acidic stretch of six residues (^{981}EDMDVA^{986}) between TM5 and TM6 is the selectivity filter for TRPM4. According to our sequence alignment, the selectivity filter of TRPM4 corresponds to the region between residues ^{1051}YEIDVC^{1056} in TRPM7 and ^{1028}GEI-DVC^{1033} in TRPM6. Different from this prediction, our data indicate the residues critical to ion selectivity in the pore region are ^{1047}EVYAYE^{1052} for TRPM7 and ^{1024}EVYAGE^{1029} for TRPM6. We demonstrate that the E1047Q mutant produced the most dramatic changes in TRPM7 channel properties. Not only does E1047Q eliminate Ca^{2+} and Mg^{2+} permeation, but it also abolishes a proton-induced increase in inward currents. Thus, the Glu^{1047} residue should be considered a key component of the selectivity filter. In addition to E1047Q, E1052Q also influenced Ca^{2+}/Mg^{2+} permeability. Furthermore, the double mutant E1047Q/E1052Q exhibited similar properties to those of E1047Q. Therefore, it is likely the Glu^{1047} and Glu^{1052} residues form a high affinity binding site for divalent cations. Asp^{1054} is a conserved residue in all TRPM channels. However, the exchange of Asp at position 1054 for Ala (D1054A) did not alter the apparent affinity for Ca^{2+} and Mg^{2+}. The negatively charged residue preceding Glu^{1047}, Asp^{1035}, has no influence on Ca^{2+} and Mg^{2+} permeability and selectivity. Therefore, our results predict that the selectivity filter of TRPM7 lies between Glu^{1047} and Glu^{1052} (or Glu^{1024}–Glu^{1029} for TRPM6).

The negatively charged residue Glu^{1047} is conserved in TRPM1, TRPM3, TRPM6, and TRPM7. Interestingly, mutation of Gln^{977} by Glu in TRPM4, the analogous residue to Glu^{1047} in TRPM7, altered the monovalent cation permeability sequence and rendered the TRPM4 pore permeable to Ca^{2+} (56), suggesting that the Glu^{1047} position is indeed crucial for determining the divalent selectivity of TRPM channels. It will be of interest to investigate whether mutation of this conserved residue influences the divalent permeability of TRPM1 and TRPM3 as well. Nonetheless, it seems that the pore structure of TRPM channels is more complicated than first imagined. For example, Oberwinkler and colleagues (57) recently identified several TRPM3 spliced variants, TRPM3α1–5. Whereas the TRPM3α-2 displays high permeability to Ca^{2+} and Mg^{2+}, TRPM3α-1, which includes an additional stretch of 12 amino acids following the invariant Asp, a residue equivalent to Asp^{1054} in TRPM7, exhibited a more than 10-fold lower permeability for divalent cations (57). This could be attributed to a possibility that the additional 12 residues result in re-arrangement of the pore structure. Because Asp^{1054} is conserved in all the TRPM channels, including both divalent permeable and monovalent selective (TRPM4 –5) ones, it may be less influential than Glu^{1047} and Glu^{1052} on divalent selectivity. Taken together, our results suggest that ^{1047}EVYAYE^{1052} in TRPM7 and ^{1024}EVY-AGE^{1029} in TRPM6 constitute the selectivity filter, and that Glu^{1047}/Glu^{1024} and Glu^{1052}/Glu^{1029} are essential for Ca^{2+}/Mg^{2+} selectivity and pH sensitivity.

Conclusions

The importance of Mg^{2+} and Ca^{2+} permeation of TRPM6 and TRPM7 has been well demonstrated. Mutations in *TRPM6* lead to familial hypomagnesemia and secondary

hypocalcemia (20, 21), and deletion of *TRPM7* causes cell death (7, 10, 22). Moreover, it has been demonstrated recently that the sensitivity of TRPM7 to external pH may contribute to the ability of the channel to control neurotransmitter release (28). In the present study, we provide strong evidence demonstrating that the amino acid residues Glu^{1024}/Glu^{1047} and Glu^{1029}/Glu^{1052} in the putative pore region of TRPM6 and TRPM7 are essential for their Ca^{2+} and Mg^{2+} permeability and pH sensitivity. These findings provide the molecular mechanisms by which TRPM6 and TRPM7 exert their physiological functions, and may in fact serve as a platform for future work aimed at discovering pharmacological agents to manipulate TRPM6 and TRPM7 channel functions. In addition, our results provide valuable information on the pore architecture of TRPM6 and TRPM7 channels, knowledge that will help guide future investigations into the complex nature of TRPM channel family members.

Addendum

After this article was submitted, and while it was being revised, we learned of a relevant paper about the molecular determinants of TRPM6 permeation (58). The results of that study also indicate that the negative charged residues are important for TRPM6 permeation properties.

Supplementary Material

Refer to Web version on PubMed Central for supplementary material.

Acknowledgments

We thank Dr. Joost G. J. Hoenderop for providing TRPM6 in the pCINeo/IRES-GFP vector; Dr. Nilius for providing TRPM4 and its mutant Q977E; Drs. David Clapham, Alan Fein, Haoxing Xu, and Dejian Ren for constructive suggestions and comments.

References

1. Harteneck C, Plant TD, Schultz G. Trends Neurosci. 2000; 23:159–166. [PubMed: 10717675]
2. Clapham DE. Nature. 2003; 426:517–524. [PubMed: 14654832]
3. Fleig A, Penner R. Novartis Found Symp. 2004; 258:248–258. 258–266. [PubMed: 15104187]
4. Schmitz C, Perraud AL, Fleig A, Scharenberg AM. Pediatr Res. 2004; 55:734–737. [PubMed: 14764909]
5. Montell C. Sci STKE. 2005; 2005:1–24.
6. Runnels LW, Yue L, Clapham DE. Science. 2001; 291:1043–1047. [PubMed: 11161216]
7. Nadler MJ, Hermosura MC, Inabe K, Perraud AL, Zhu Q, Stokes AJ, Kurosaki T, Kinet JP, Penner R, Scharenberg AM, Fleig A. Nature. 2001; 411:590–595. [PubMed: 11385574]
8. Voets T, Nilius B, Hoefs S, van der Kemp AWCM, Droogmans G, Bindels RJM, Hoenderop JGJ. J Biol Chem. 2004; 279:19–25. [PubMed: 14576148]
9. Chubanov V, Waldegger S, Mederos y Schnitzler M, Vitzthum H, Sassen MC, Seyberth HW, Konrad M, Gudermann T. Proc Natl Acad Sci U S A. 2004; 101:2894–2899. [PubMed: 14976260]
10. Schmitz C, Dorovkov MV, Zhao X, Davenport BJ, Ryazanov AG, Perraud AL. J Biol Chem. 2005; 280:37763–37771. [PubMed: 16150690]
11. Li M, Jiang J, Yue L. J Gen Physiol. 2006; 127:525–537. [PubMed: 16636202]
12. Monteilh-Zoller MK, Hermosura MC, Nadler MJ, Scharenberg AM, Penner R, Fleig A. J Gen Physiol. 2003; 121:49–60. [PubMed: 12508053]
13. Kozak JA, Cahalan MD. Biophys J. 2003; 84:922–927. [PubMed: 12547774]
14. Kozak JA, Matsushita M, Nairn AC, Cahalan MD. J Gen Physiol. 2005; 126:499–514. [PubMed: 16260839]
15. Kozak JA, Cahalan MD. Biophys J. 2004; 86:63. (abstr.).

16. Hermosura MC, Monteilh-Zoller MK, Scharenberg AM, Penner R, Fleig A. J Physiol. 2002; 539:445–458. [PubMed: 11882677]
17. Runnels LW, Yue L, Clapham DE. Nat Cell Biol. 2002; 4:329–336. [PubMed: 11941371]
18. Takezawa R, Schmitz C, Demeuse P, Scharenberg AM, Penner R, Fleig A. Proc Natl Acad Sci U S A. 2004; 101:6009–6014. [PubMed: 15069188]
19. Jiang J, Li M, Yue L. J Gen Physiol. 2005; 126:137–150. [PubMed: 16009728]
20. Walder RY, Landau D, Meyer P, Shalev H, Tsolia M, Borochowitz Z, Boettger MB, Beck GE, Englehardt RK, Carmi R, Sheffield VC. Nat Genet. 2002; 31:171–174. [PubMed: 12032570]
21. Schlingmann KP, Weber S, Peters M, Niemann Nejsum L, Vitzthum H, Klingel K, Kratz M, Haddad E, Ristoff E, Dinour D, Syrrou M, Nielsen S, Sassen M, Waldegger S, Seyberth HW, Konrad M. Nat Genet. 2002; 31:166–170. [PubMed: 12032568]
22. Schmitz C, Perraud AL, Johnson CO, Inabe K, Smith MK, Penner R, Kurosaki T, Fleig A, Scharenberg AM. Cell. 2003; 114:191–200. [PubMed: 12887921]
23. Chubanov V, Gudermann T, Schlingmann KP. Pflügers Arch. 2005; 451:228–234.
24. Aarts M, Iihara K, Wei WL, Xiong ZG, Arundine M, Cerwinski W, MacDonald JF, Tymianski M. Cell. 2003; 115:863–877. [PubMed: 14697204]
25. Su LT, Agapito MA, Li M, Simonson WT, Huttenlocher A, Habas R, Yue L, Runnels LW. J Biol Chem. 2006; 281:11260–11270. [PubMed: 16436382]
26. Clark K, Langeslag M, van Leeuwen B, Ran L, Ryazanov AG, Figdor CG, Moolenaar WH, Jalink K, van Leeuwen FN. EMBO J. 2006; 25:290–301. [PubMed: 16407977]
27. Elizondo MR, Arduini BL, Paulsen J, MacDonald EL, Sabel JL, Henion PD, Cornell RA, Parichy DM. Curr Biol. 2005; 15:667–671. [PubMed: 15823540]
28. Krapivinsky G, Mochida S, Krapivinsky L, Cibulsky SM, Clapham DE. Neuron. 2006; 52:485–496. [PubMed: 17088214]
29. Yue L, Navarro B, Ren D, Ramos A, Clapham D. J Gen Physiol. 2002; 160:845–853. [PubMed: 12451053]
30. Jordt SE, Tominaga M, Julius D. Proc Natl Acad Sci U S A. 2000; 97:8134–8139. [PubMed: 10859346]
31. Askwith CC, Wemmie JA, Price MP, Rokhlina T, Welsh MJ. J Biol Chem. 2004; 279:18296–18305. [PubMed: 14960591]
32. Yermolaieva O, Leonard AS, Schnizler MK, Abboud FM, Welsh MJ. Proc Natl Acad Sci U S A. 2004; 101:6752–6757. [PubMed: 15082829]
33. Hille, B. Ion Channels of Excitable Membranes. 3. Sinauer Associates, Inc; Sunderland, MA: 2003.
34. Yue L, Peng JB, Hediger MA, Clapham DE. Nature. 2001; 410:705–709. [PubMed: 11287959]
35. Kerschbaum HH, Kozak JA, Cahalan MD. Biophys J. 2003; 84:2293–2305. [PubMed: 12668438]
36. Kerschbaum HH, Cahalan MD. J Gen Physiol. 1998; 111:521–537. [PubMed: 9524136]
37. Tikhonov DB, Magazanik LG. J Membr Biol. 1998; 161:1–8. [PubMed: 9430616]
38. Ellinor PT, Yang J, Sather WA, Zhang JF, Tsien RW. Neuron. 1995; 15:1121–1132. [PubMed: 7576655]
39. Demeuse P, Penner R, Fleig A. J Gen Physiol. 2006; 127:421–434. [PubMed: 16533898]
40. Vennekens R, Hoenderop JGJ, Prenen J, Stuiver M, Willems PHGM, Droogmans G, Nilius B, Bindels RJM. J Biol Chem. 2000; 275:3963–3969. [PubMed: 10660551]
41. Vennekens R, Prenen J, Hoenderop JG, Bindels RJ, Droogmans G, Nilius B. Pflügers Arch. 2001; 442:237–242.
42. Yeh BI, Sun TJ, Lee JZ, Chen HH, Huang CL. J Biol Chem. 2003; 278:51044–51052. [PubMed: 14525991]
43. Nilius B, Vennekens R, Prenen J, Hoenderop JG, Droogmans G, Bindels RJ. J Biol Chem. 2001; 276:1020–1025. [PubMed: 11035011]
44. Garcia-Martinez C, Morenilla-Palao C, Planells-Cases R, Merino JM, Ferrer-Montiel A. J Biol Chem. 2000; 275:32552–32558. [PubMed: 10931826]

45. Suzuki M, Mizuno A, Kodaira K, Imai M. J Biol Chem. 2003; 278:22664–22668. [PubMed: 12692122]
46. Voets T, Prenen J, Vriens J, Watanabe H, Janssens A, Wissenbach U, Bodding M, Droogmans G, Nilius B. J Biol Chem. 2002; 277:33704–33710. [PubMed: 12093812]
47. Liu D, Zhang Z, Liman ER. J Biol Chem. 2005; 280:20691–20699. [PubMed: 15731110]
48. Chen XH, Bezprozvanny I, Tsien RW. J Gen Physiol. 1996; 108:363–374. [PubMed: 8923262]
49. Chen XH, Tsien RW. J Biol Chem. 1997; 272:30002–30008. [PubMed: 9374474]
50. Woodhull AM. J Gen Physiol. 1973; 61:687–708. [PubMed: 4541078]
51. Owsianik G, Talavera K, Voets T, Nilius B. Annu Rev Physiol. 2006; 68:685–717. [PubMed: 16460288]
52. Launay P, Fleig A, Perraud AL, Scharenberg AM, Penner R, Kinet JP. Cell. 2002; 109:397–407. [PubMed: 12015988]
53. Liu D, Liman ER. Proc Natl Acad Sci U S A. 2003; 100:15160–15165. [PubMed: 14657398]
54. Prawitt D, Monteilh-Zoller MK, Brixel L, Spangenberg C, Zabel B, Fleig A, Penner R. Proc Natl Acad Sci U S A. 2003; 100:15166–15171. [PubMed: 14634208]
55. Hofmann T, Chubanov V, Gudermann T, Montell C. Curr Biol. 2003; 13:1153–1158. [PubMed: 12842017]
56. Nilius B, Prenen J, Janssens A, Owsianik G, Wang C, Zhu MX, Voets T. J Biol Chem. 2005; 280:22899–22906. [PubMed: 15845551]
57. Oberwinkler J, Lis A, Giehl KM, Flockerzi V, Philipp SE. J Biol Chem. 2005; 280:22540–22548. [PubMed: 15824111]
58. Topala CN, Groenestege WT, Thebault S, van den Berg D, Nilius B, Hoenderop JG, Bindels RJ. Cell Calcium. 2007; 41:513–523. [PubMed: 17098283]

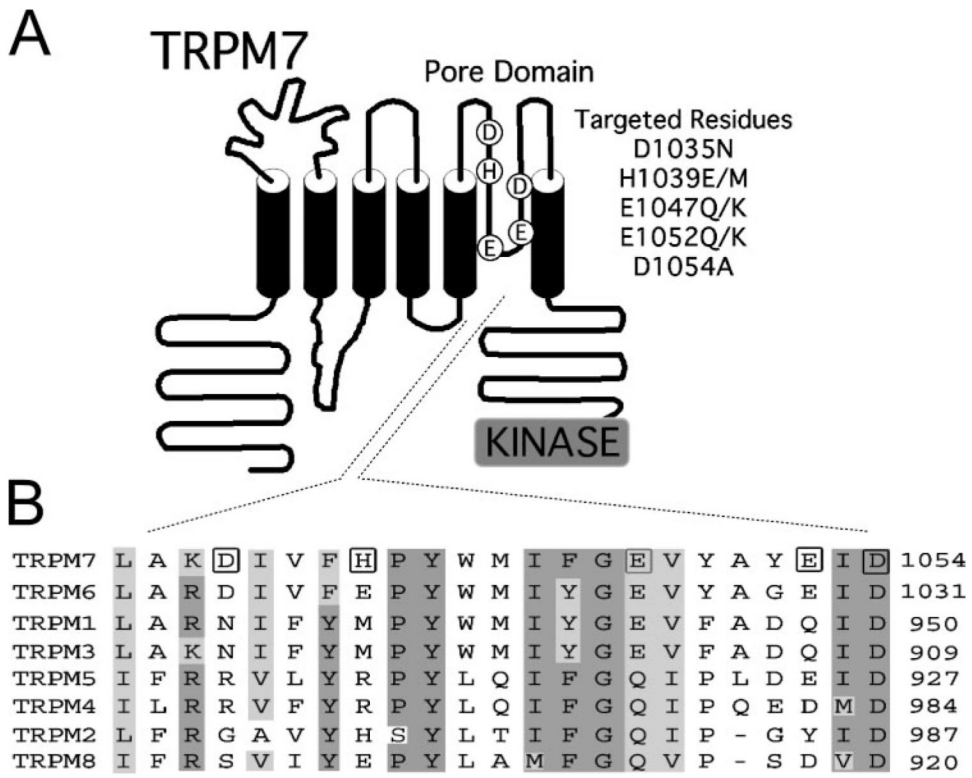

FIGURE 1. Alignment of TRPM7 pore region with other TRPM channels

A, schematic structure of the TRPM7 and positions of substituted amino acid residues in the TRPM7 channel. *B*, alignment of pore region of TRPM channels. Amino acids in *boxes* are the ones that were selected for analysis. The GenBank™ accession numbers of the mouse TRPM7, human TRPM1– 6, and TRPM8 are AF376052, AAC8000, AAI12343; NP_060106, NP_055370, Q9BX84; and NP_076985, respectively.

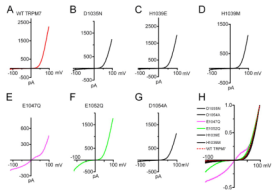

FIGURE 2. Current-voltage relationships of WT TRPM7 and its mutants

A–G, representative currents elicited by ramp protocols ranging from −120 to +100 mV in WT TRPM7 and its mutants. Note the significant changes in the I–V relation of E1047Q (*E*) and E1052Q (*F*). *H*, normalized I–V curves of WT TRPM7 and its mutants. The I–V curves of D1035N, H1039E, H1039M, and D1054A show outward rectification, and are superimposed with that of WT TRPM7; whereas E1047Q exhibits double-rectification with significantly increased inward currents and markedly decreased outward currents. Inward current of E1052Q is substantially larger than that of WT TRPM7.

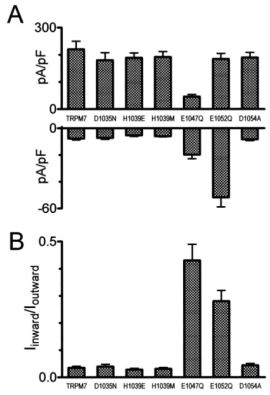

FIGURE 3. Average current amplitudes of WT TRPM7 and its mutants

A, mean outward(*top*)and inward (*bottom*)current amplitudes measured at +100 and −120 mV, respectively(n =8).*B*, ratios of inward *versus* outward current amplitude (n =8).

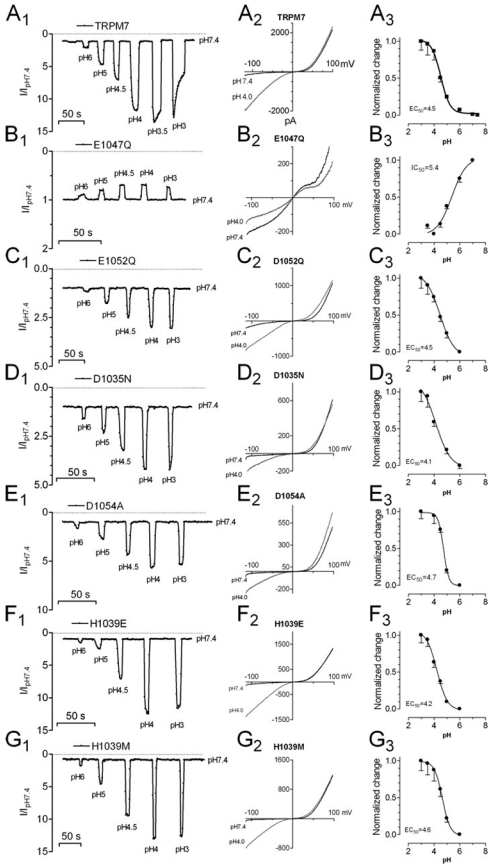

FIGURE 4. Effects of acidic pH on WT TRPM7 and its mutants

A$_1$*–G*$_1$, changes in the inward currents by acidification of external solutions. Current amplitudes were measured at −120 mV at the indicated pH and normalized to the amplitude obtained at pH 7.4. Note that E1047Q currents were inhibited by acidic pH solutions, with maximal inhibition of ~30% at pH 4.0. *A*$_2$*–G*$_2$, representative recordings of WT TRPM7 and its mutants obtained in the external solutions at pH 7.4 and 4.0. *A*$_3$*–G*$_3$, concentration-dependent effects of protons on WT TRPM7 and its mutants. The changes in current amplitude at the indicated pH were normalized to the maximal change in current amplitude. Average data were fitted with the Hill equation with average parameters obtained from best fits to individual cells. The 50% potentiation pH ($pH_{1/2}$) and Hill coefficient were $pH_{1/2}$ = 4.5 ± 0.5 (n_H = 1.2, n = 7) for WT TRPM7; $pH_{1/2}$ = 4.1 ±0.2 (n_H = 0.8, n =5) for D1035N; $pH_{1/2}$ = 4.5 ± 0.4 (n_H = 0.9, n = 5) for E1052; $pH_{1/2}$ = 4.7 ± 0.8 (n_H = 2.1, n = 6) for D1054A; $pH_{1/2}$ = 4.2 ± 0.4 (n_H = 1.1, n = 9) for H1039E; and $pH_{1/2}$ = 4.6 ±0.6 (n_H = 1.4, n =8) for H1039M; respectively. E1047Q inward currents were blocked by low pH, with the 50% inhibition pH of $pH_{1/2}$ = 5.4 ±0.7 (n_H = 0.9, n = 5).

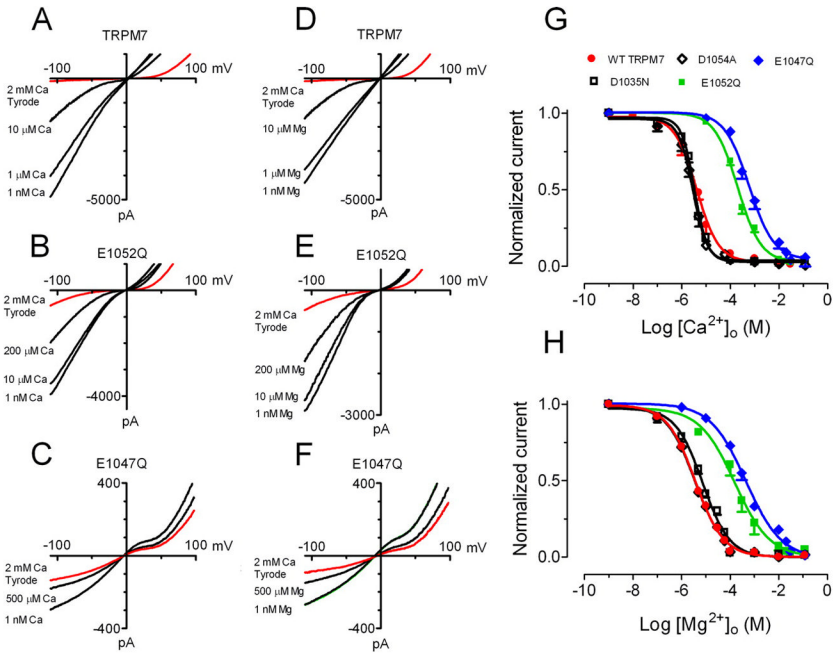

FIGURE 5. Changes in affinity of Ca^{2+} and Mg^{2+} in TRPM7 mutants

A–C, representative recordings of WT TRPM7, E1052Q, and E1047Q obtained in the external solutions containing 1 nM (DVF), 1, 10, 200, and 500 μM Ca^{2+}, and in 2 mM Ca^{2+} Tyrode solutions, respectively. *D–F*, typical currents of WT TRPM7, E1052Q, and E1047Q recorded in 1 nM, 1, 10, 200, or 500 μM Mg^{2+} containing solutions, and in 2 mM Ca^{2+} Tyrode solution, respectively. *G* and *H*, dose-response curves of Ca^{2+} and Mg^{2+} for WT TRPM7 and its mutants. The IC_{50} values obtained by best fit with the Hill equation for the Ca^{2+} block were (μM): 4.1 ± 0.2 (n_H =0.96, n = 10) for WT TRPM7, 3.3 ± 0.1 (n_H = 1.7, n = 7) for D1035N, 593.6 ± 69.9 (n_H = 0.8, n = 5) for E1047Q, 202.2 ± 14.3 (n_H = 0.9, n = 7) for E1052Q, and 2.9 ± 1.3 (n_H =1.5, n =8) for D1054A, respectively. The IC_{50} values for Mg^{2+} block were (μM): 3.6±0.4 (n_H = 0.7, n = 8) for TRPM7, 7.4± 0.8(n_H = 0.8, n= 7) for D1035N, 442.9 ± 53.6 (n_H = 0.6, n = 6) for E1047Q, 154.7 ± 23.4 (n_H = 0.6, n = 6) for E1052Q, and 3.6 ± 0.2 (n_H = 0.7, n = 8) for D1054A, respectively.

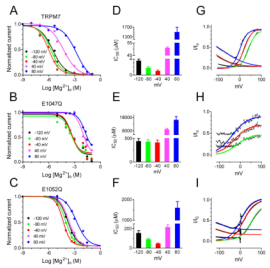

FIGURE 6. Voltage-dependent effects of Mg^{2+} on monovalent currents of WT TRPM7, E1047Q, and E1052Q

A–C, dose-response curves for the inhibition of inward monovalent currents by Mg^{2+} at the indicated voltages for WT TRPM7 (*A*), E1047Q (*B*), and E1052Q (*C*). *D–F*, the IC_{50} values obtained by best fit with the Hill equation at various voltages (n = 8 for TRPM7; n = 6 for E1047Q and E1052Q, respectively). *G–I*, current ratios (I/I_0) of TRPM7 (*G*), E1047Q (*H*), and E1052Q (*I*) in the presence of various Mg^{2+} concentrations, respectively. Note the relief of Mg^{2+} block at hyperpolarized potentials observed in TRPM7 and E1052Q, but not in E1047Q. *Dotted lines* represent I/I_0, where I is the current in the presence of Mg^{2+}, and I_0 is the current in DVF solution. *Solid lines* represent the best fit of the current ratio to the Boltzmann functions (see “Experimental Procedures”). In *G*, for the voltage-dependent block on TRPM7, $V_{0.5}$ values for 3 (*blue*), 10 (*red*), and 100 (*green*) μM Mg^{2+} were 0.3, 20.9, and 40.6 mV, respectively; the values of k(*depol*) were almost identical, with 15.2 mV at 3 μM Mg^{2+}, 15.5 mV at 10 μM Mg^{2+}, and 15.6 mV at 100 μM Mg^{2+}, respectively; for the voltage-dependent relief of block on TRPM7, $V_{0.5}$ for 3 and 10 μM Mg^{2+} were −64.9 and −124.2 mV, respectively, and the values of k(*hyperpol*) were 49.8 and 50.4 mV, respectively. In *H*, Boltzmann fit of the voltage-dependent block on E1047Q at 500 μM (*blue*), 10 mM (*red*), and 20 mM(*green*) Mg^{2+} generated $V_{0.5}$ values of −39.3, −27.5, and −16.3 mV, respectively; and k(*depol*) values of 36.2, 35.8, and 35.6 mV, respectively. In *I*, for voltage-dependent block on E1052Q at 150 μM (*blue*), 1 mM (*red*), and 5 mM (*green*) Mg^{2+}, the $V_{0.5}$ values were 2.5, 15.2, and 50.6 mV, respectively; and k(*depol*) values were 24.5, 24.3, and 24.4 mV, respectively. For voltage-dependent relief of Mg^{2+} block on E1052Q, the $V_{0.5}$ values were −87.7 and −95.4 mV at 150 μM, and 1 mM Mg^{2+}, respectively, and k(*hyperpol*) values were 29.1 and 29.0 mV at 150 μM and 1 mM Mg^{2+}, respectively. The fraction of the membrane electrical field δ_{out} calculated from k(*depol*) based on $k = RT/z\delta F$ was 0.84 for TRPM7, 0.36 for E1047Q, and 0.52 for E1052Q, respectively (see supplementary materials Table S2).

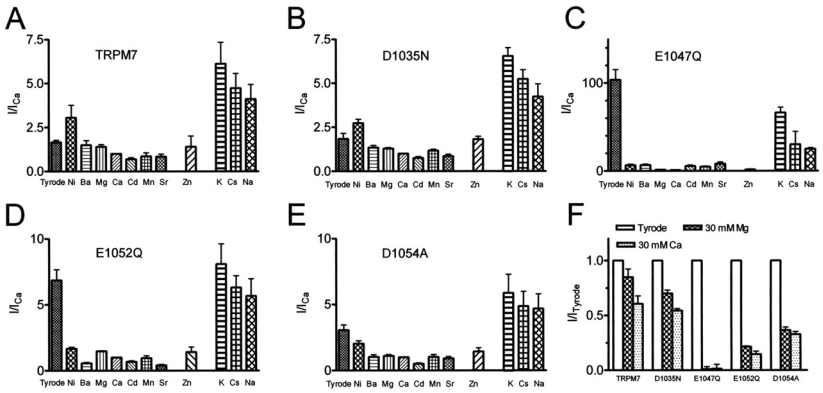

FIGURE 7. Changes in divalent permeability of TRPM7 mutants (mean ±S. E.,*n* =6)

A–E, currents recorded under the indicated conditions were normalized to the current amplitude value obtained in 30 mM Ca^{2+} external solutions. The sequence of monovalent permeability was not changed (K^+>Cs^+>Na^+) in the mutants compared with WT TRPM7; however, the monovalent permeabilities in E1047Q were significantly larger than that of WT TRPM7. *F*, currents obtained in 30 mM Ca^{2+} or Mg^{2+} were normalized to the current amplitude obtained in Tyrode solution. Note that the ratios of I_{Ca}/I_{Tyrode} and I_{Mg}/I_{Tyrode} for E1047Q were 0.014 and 0.0096, respectively. The $I_{Ca(E1047Q)}/I_{Ca(TRPM7)}$ was 0.023, and $I_{Mg(E1047Q)}/I_{Mg(TRPM7)}$ was 0.011, respectively.

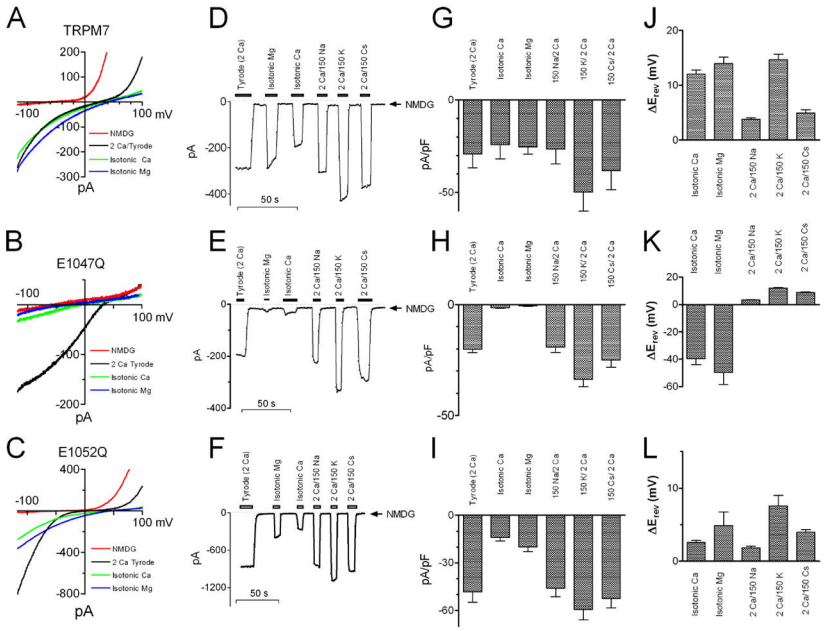

FIGURE 8. E1047Q diminishes Ca^{2+} permeation and eliminates Mg^{2+} permeation

A–C, representative currents of TRPM7, E1047Q, and E1052Q elicited by ramp protocols in 2 mM Ca^{2+}/Tyrode, NMDG, isotonic Ca^{2+}, and isotonic Mg^{2+} solutions, respectively. P2 pipette solution containing reduced Cs^{+} concentration (10 mM) was used. *D–F*, inward currents measured at −120 mV under different conditions in the representative cells for TRPM7 (*D*), E1047Q (*E*), and E1052Q (*F*). *G–I*, average current amplitudes (mean ±S.E., *n* =6) measured at −120 mV under the indicated conditions for TRPM7, E1047Q, and E1052Q. *J–L*, changes in reversal potentials of TRPM7 (*J*), E1047Q (*K*), and E1052Q (*L*) (mean ± S.E., *n* =6). ΔE_{rev} was obtained by subtracting the reversal potential under indicated conditions by the reversal potential in Tyrode solution.

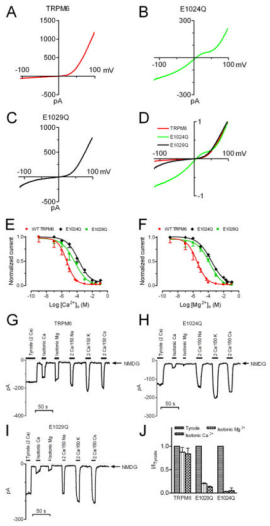

FIGURE 9. Changes in Ca^{2+} and Mg^{2+} permeability in TRPM6 mutants E1024Q and E1029Q

A–C, current-voltage relations for TRPM6, E1029Q, and E1024Q elicited by voltage ramps ranging from −120 to +100 mV. *D*, normalized I–V curves of TRPM6, E1029Q, and E1024Q. *E* and *F*, dose-response curves of Ca^{2+} and Mg^{2+} for TRPM6 and its mutants. The IC_{50} values obtained by best fit with the Hill equation for the Ca^{2+} block (*E*) were (μM): 4.6± 0.4 (n_H = 0.8, *n* =10) for TRPM6, 153.5 ± 20.0 (n_H=0.6, *n* =5) for E1024Q, and 50.5 ±9.0 (n_H =0.5, *n* =5) for E1029Q, respectively. The IC_{50} values for Mg^{2+} block were (μM): 3.4 ±0.3 (n_H = 0.7, *n* =8) for TRPM6, 237.2 ±26.2 (n_H = 0.5, *n* =6) for E1024Q, and 149.2 ±19.2 (n_H = 0.6, *n* =6) for E1029Q, respectively. *G–I*, inward current amplitude of TRPM6, E1024Q, and E1029Q measured at −120 mV under the indicated conditions. *J*, average current amplitudes of TRPM6, E1024Q, and E1029Q obtained in isotonic Ca^{2+} and Mg^{2+} solutions (120 mM) normalized to the current amplitude obtained in Tyrode solution.

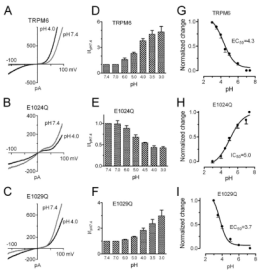

FIGURE 10. Effects of external protons on TRPM6 and its mutants E1024Q and E1029Q

A–C, representative recordings of TRPM6 (*A*), E1024Q (*B*), and E1029Q (*C*) obtained in the external solutions at pH 7.4 and 4.0. Note that E1024Q currents were blocked by low pH (*B*). *D–F*, changes in inward current amplitude measured at −120 mV at the indicated pH values. *G–I*, concentration-dependent effects of protons on TRPM6 (*G*), E1024Q (*H*), and E1029Q (*I*). Average data were fitted with the Hill equation with average parameters obtained from best fits to individual cells. The 50% potentiation pH ($pH_{1/2}$) and Hill coefficient were $pH_{1/2}$ = 4.3 ±0.4, n_H = 0.7 (*n* =8) for TRPM6, and $pH_{1/2}$ = 3.7 ±0.2, n_H = 1.0 (*n* =5) for E1029Q, respectively; and the 50% inhibition pH ($pH_{1/2}$) and Hill coefficient were $pH_{1/2}$ = 5.0 ± 0.7, n_H = 0.5 (*n* = 5) for E1024Q.

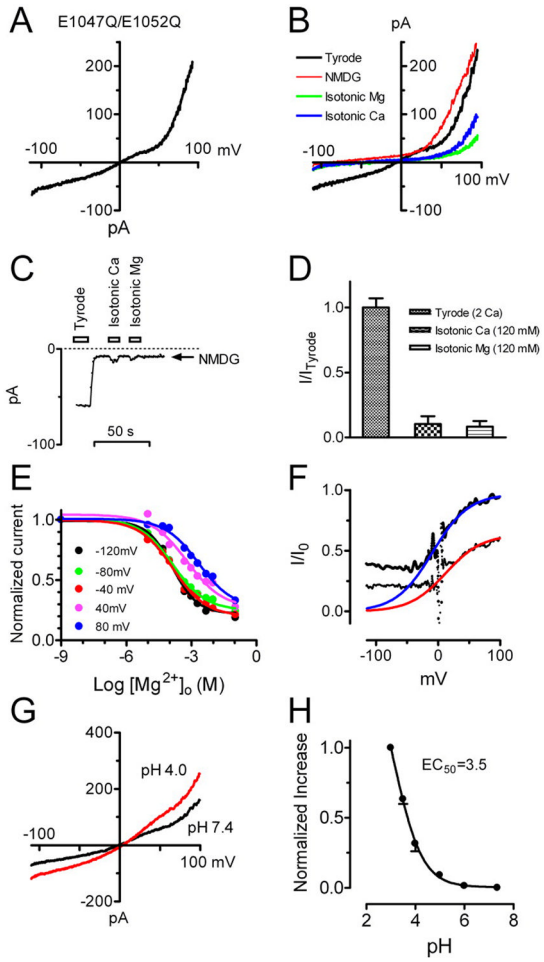

FIGURE 11. Changes in Mg^{2+} and Ca^{2+} permeability and pH sensitivity in the double mutant E1047Q/E1052Q of TRPM7

A, typical recording of the E1047Q/E1052Q current elicited by a voltage ramp protocol ranging from −120 to +100 mV. *B*, currents of E1047Q/E1052Q recorded in Tyrode, NMDG, isotonic Ca^{2+} and Mg^{2+} (120 mM) solutions. Note the diminished inward currents in isotonic Ca^{2+} and Mg^{2+} solutions. *C*, inward current amplitude measured at −120 mV under various conditions. *D*, average current amplitudes at −120 mV in isotonic Ca^{2+} and Mg^{2+} solutions normalized to the current amplitude in the Tyrode solution. The current amplitude of E1047Q/E1052Q in isotonic Ca^{2+} and Mg^{2+} (120 mM) solutions was 0.1 ±0.06 and 0.08 ±0.04 (n = 6) of that in Tyrode solution, respectively. *E*, concentration-dependent effects of Mg^{2+} on E1047Q/E1052Q at various voltages. The IC_{50} values of Mg^{2+} were 132.7 ±25.6 μM at −120 mV, 135.2 ±17.3 μM at −80 mV, 138.4 ±41.3 μM at −40 mV, 632.3 ±76.7 μM at +40 mV, and 2.2± 0.4 mM at +80 mV, respectively (n =5). *F*, current ratio I/I_0 at 100 μM and 2 mM Mg^{2+} plotted as a function of membrane potential. The best fit with the Boltzmann equation for voltage-dependent block of Mg^{2+} at 100 μM and 2 mM yielded the V_{50} values of −9.6 and 12.3 mV, respectively; and k values of 29.3 and 29 mV, respectively. The fraction of the membrane electrical field δ_{out} calculated based on $k = RT/z\delta F$ was 0.44. *G*, effects of external protons on E1047Q/E1052Q. Inward current amplitude was increased by ~32% at pH 4.0. *H*, concentration-dependent effects of protons on E1047Q/E1052Q. The best fit with the Hill equation yielded $pH_{1/2}$ of 3.5 ±0.1 (n_H = 0.7, n = 5).